Moving Targets Imaging in Spaceborne TOPS SAR

Hongbo Mo [1], Wei Xu [2], and Zhimin Zeng [1]

[1] School of Information and Communication Engineering and Beijing Key Laboratory of Network System Architecture and Convergence
Beijing University of Posts and Telecommunications, Beijing, 100876, China
mohongbo@bupt.edu.cn, zengzm@bupt.edu.cn

[2] Spaceborne Microwave Remote Sensing System Department
Institute of Electronics, Chinese Academy of Sciences (IECAS), Beijing, 100190, China
iecasxuwei@163.com

Abstract ─ Terrain Observation by Progressive Scans (TOPS) is the spaceborne wide swath synthetic aperture radar (SAR) imaging mode and attractive for ocean remote sensing. Its imaging processors are quite different from the one of the conventional stripmap mode due to antenna beam progressive scanning. This paper proposes a new imaging processor in TOPS for moving targets especially for moving ships in ocean. In addition to resolving the azimuth aliasing problem in TOPS, the Doppler parameter estimation is the key point of the proposed processor. According to the estimated Doppler parameters, some transfer functions of the processor should be updated. Simulation results on point and distributed targets validate the proposed imaging processor.

Index Terms ─ Doppler parameter estimation, moving target imaging, Synthetic Aperture Radar (SAR), Terrain Observation by Progressive Scans (TOPS).

I. INTRODUCTION

The terrain observation by progressive scans (TOPS) mode achieves the wide swath coverage by progressive steering the antenna beam in both azimuth and elevation, and it was first successfully achieved by the TerraSAR-X (TSX) in 2008 [1, 2]. Although the wide swath coverage of the TOPS is exchanged by the impaired azimuth resolution compared with the stripmap case, the TOPS imaging scheme is the attractive spaceborne synthetic aperture radar (SAR) imaging mode for multiple applications, especially for ocean observation and ships detection due to its wide swath coverage with better system performances than conventional ScanSAR [2]. Therefore, most of future spaceborne microwave remote sensing missions would adopt this wide swath imaging mode for ocean remote sensing [2].

Since the azimuth antenna beam is steered from aft to fore during the whole raw data acquisition duration, the raw data of the TOPS mode couldn't be well handled by conventional stripmap processors. Up to now, multiple imaging efficient processors are proposed for the TOPS mode [1, 3-7]. However, little work about moving targets focusing in TOPS could be found. In this paper, a new imaging processor to handle the raw data of moving targets especially for moving ships in ocean in TOPS is proposed. In addition to resolve both Doppler spectra and azimuth output SAR image back folding problems, the key point of the proposed imaging processor is the Doppler parameters estimation in TOPS. With the estimated Doppler parameters, the processor is modified to be fit for the signal mode of the moving target.

This paper is arranged as follows. The echo model of moving targets in TOPS is established in Section II. The proposed imaging processor for moving targets in TOPS is presented in detail in Section III. To validate the proposed imaging algorithm, a simulation experiment on point targets is carried out. Finally, this paper is concluded in section V.

II. ECHO PROPERTIES OF MOVING TARGETS IN TOPS

In TOPS, the elevation antenna beam is periodically scanned from sub-swath to sub-swath to obtain the wide swath coverage similar to ScanSAR, while the azimuth antenna beam is actively steered from aft to fore during the whole SAR raw data acquisition time as shown in Fig. 1. In Fig. 1, v_s is the velocity of the sensor, and ω_r is the azimuth beam rotation rate. In addition to making sure azimuth continuous imaging in each sub-swath, the azimuth beam progressive scanning is adopted to reduce the effect of the scalloping phenomenon in the burst imaging mode, since each target is illuminated by the whole 3dB azimuth antenna pattern in TOPS. The better image quality in TOPS than in ScanSAR is very attractive, especially for ocean remote sensing applications, as the

Submitted On: May 29, 2016
Accepted On: September 9, 2016

scalloping effect of SAR images of ocean is hard to correct by existing radiometric calibration algorithms [2].

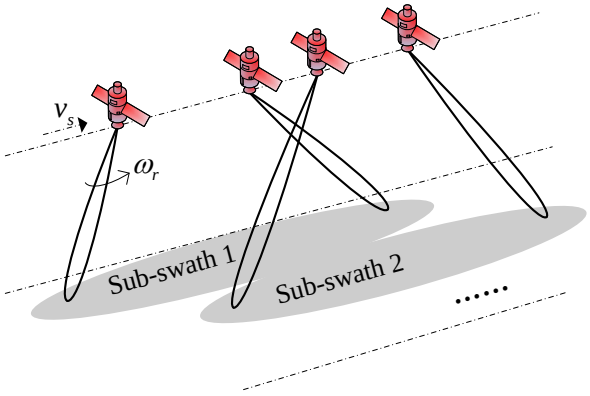

Fig. 1. TOPS SAR acquisition geometry.

The planar imaging geometry of the TOPS mode in a sub-swath is shown in Fig. 2, which indicates that the azimuth beam is electronically steered from aft to fore. As show in Fig. 2, there is a fixed virtual rotation center on the imaging plane, and the rotation center is farther away from the imaged scene than the SAR sensor. The rotation range r_{rot} has negative sign, and v_r is the effective velocity of the sensor in the planar imaging geometry. Assuming that there is a moving target P with the azimuth location x and the slant range r in the scene, and the moving target velocity is u. Furthermore, the moving target velocity is divided into two components: the azimuth velocity component u_a and the range velocity component u_r, as shown in Fig. 2.

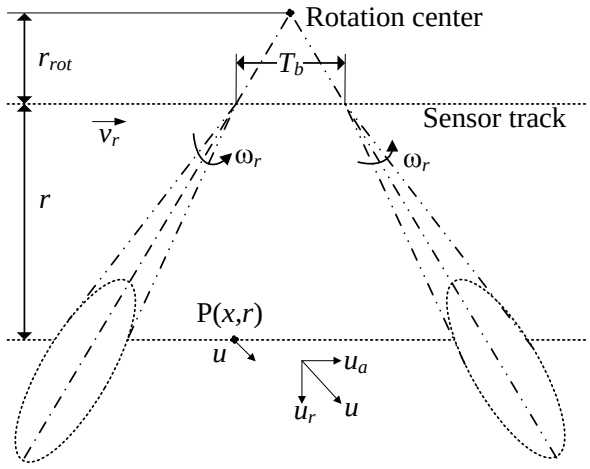

Fig. 2. Planar TOPS SAR geometry in a sub-swath.

The echo signal of a point moving target P as shown in Fig. 2 can be expressed as [8-10]:

$$s(\tau,t;x,r)=C_0\cdot\exp\left(-j\frac{4\pi}{\lambda}R(t)\right)\cdot\mathrm{rect}\left[\frac{\tau-2R(t)/c}{\tau_p}\right]\cdot\exp\left[-jK_r\left(\tau-\frac{2R(t)}{c}\right)^2\right]\cdot\mathrm{rect}\left[\frac{A(r)\cdot t-x/(v_r-u_a)}{T_f}\right], \quad (1)$$

with

$$R(t)=\sqrt{(v_r t-u_a t-x)^2+(r+u_r t)^2}, \quad (2)$$

$$A(r)=1+\frac{\omega_r\cdot r}{v_r-u_a}, \quad (3)$$

where τ and t are the range time and the azimuth time, respectively, C_0 is a complex constant, λ is the wavelength, K_r is the chirp rate of the transmitted pulse, c is the light speed, τ_p is the transmitted pulse duration, and T_f is the synthetic aperture time in the stripmap mode determined by the exploited azimuth beam angular interval. Compared to echoes of moving targets in the conventional stripmap mode, the major difference in TOPS is the azimuth signal component. Therefore, we just need to focus on analyzing the properties of the azimuth signal, and the simplified expression of the azimuth signal component of point target P(x, r) is expressed as follows:

$$s_a(t;x,r)=C_1\cdot\exp\left(-j\frac{4\pi}{\lambda}R(t)\right)\cdot\mathrm{rect}\left[\frac{A(r)\cdot t-x/v}{T_f}\right]\approx C_2\cdot\exp\left(-j\frac{4\pi r}{\lambda}\right)\cdot\mathrm{rect}\left[\frac{A(r)\cdot t-x/v}{T_f}\right]\cdot\exp\left[-j\pi\frac{2(v^2+u_r^2)t^2}{\lambda r}+j\frac{4\pi}{\lambda}\left(\frac{vx}{r}-u_r\right)t\right], \quad (4)$$

where both C_1 and C_2 are complex constants, while $v=v_r-u_a$ is the relative azimuth velocity between the SAR sensor and the moving target. According to (4), the instantaneous Doppler frequency $f_a(t;x,r)$ of the moving target P could be obtained as follows:

$$f_a(t;x,r)=\frac{1}{2\pi}\cdot\frac{\partial\varphi(t)}{\partial t}=-\frac{2(v^2+u_r^2)}{\lambda r}t+\frac{2}{\lambda}\left(\frac{vx}{r}-u_r\right). \quad (5)$$

Furthermore, according to the last component of (1), the azimuth beam illumination center time for the moving target P is:

$$t_x=\frac{x}{A(r)\cdot v}. \quad (6)$$

Consequently, the Doppler centroid of the moving target could be obtained as:

$$f_{dc}(x,r) = f_a(t_x;x,r) = \frac{2v^2}{\lambda r}\cdot\frac{x}{v}\cdot\frac{A(r)-1}{A(r)} - \frac{2u_r^2}{\lambda r}\cdot\frac{x}{A(r)\cdot v} - \frac{2u_r}{\lambda} = \frac{2v^2}{\lambda r_{rot}}\cdot\frac{x}{A(r)\cdot v} - \frac{2u_r^2}{\lambda r}\cdot\frac{x}{A(r)\cdot v} - \frac{2u_r}{\lambda}. \quad (7)$$

The Doppler centroid $f_{dc}(x,r)$ of the moving target P includes three parts. The first part is almost the same as the fixed target in TOPS; the second part due to the range velocity u_r of the moving target is very small and could be neglected; the third part is also caused by the velocity u_r but much larger than the second part. From (5), the Doppler modulation rate of the moving target P is:

$$k_{am}(x,r) = \frac{\partial f_a(t;x,r)}{\partial t} \approx -\frac{2(v^2+u_r^2)}{\lambda r}. \quad (8)$$

Figure 3 shows the azimuth time frequency diagram (TFD) in TOPS for both fixed and moving targets, the thick solid and the thick dash lines indicates fixed and moving targets, respectively. As shown in Fig. 3, the fixed target Q and the moving target P are with the same azimuth location at the moment of the azimuth beam center time, and the Doppler frequency difference Δf_a between their Doppler centroids is expressed as follows:

$$\Delta f_{ac}(x,r) = f_{dc}(x,r) - f_{ac}(x,r) \approx -\frac{2u_a}{\lambda r_{rot}}\cdot\frac{x}{A(r)} - \frac{2u_r}{\lambda} \approx -\frac{2u_r}{\lambda}, \quad (9)$$

where $f_{ac}(x,r)$ is the Doppler centroid of the fixed target with the location of (x, r). Therefore, the Doppler frequency difference Δf_a is mainly determined by the range velocity component u_r of the moving target.

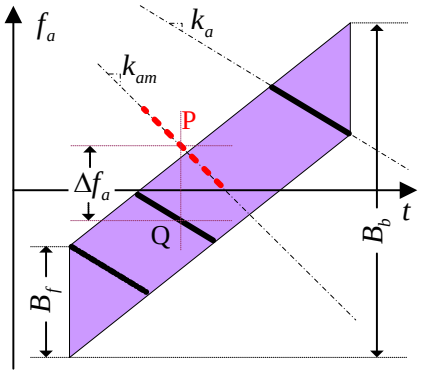

Fig. 3. The azimuth time frequency diagram in TOPS for both fixed and moving targets.

III. NEW IMAGING PROCESSOR FOR MOVING TARGETS IN TOPS

In the TOPS mode, the Doppler bandwidth of the whole burst may span over several pulse repetition frequency (PRF) intervals, multiple approaches to overcome this problem have been proposed in recent years [3-7]. Among them, the azimuth pre-filtering based on the two step focusing technique is one of most efficient approaches, which introduces an azimuth involution between the SAR raw data and the selected chirp signal and is implemented by two complex multiplications and an azimuth Fourier transform (FT). In this paper, we extend the azimuth pre-filtering approach based on the two step focusing technique to handle the raw data of moving targets in TOPS. The key point of the extended imaging algorithm is the updated selected transfer functions for SAR focusing according to the target velocity estimation results. The block diagram of the proposed is shown in Fig. 4.

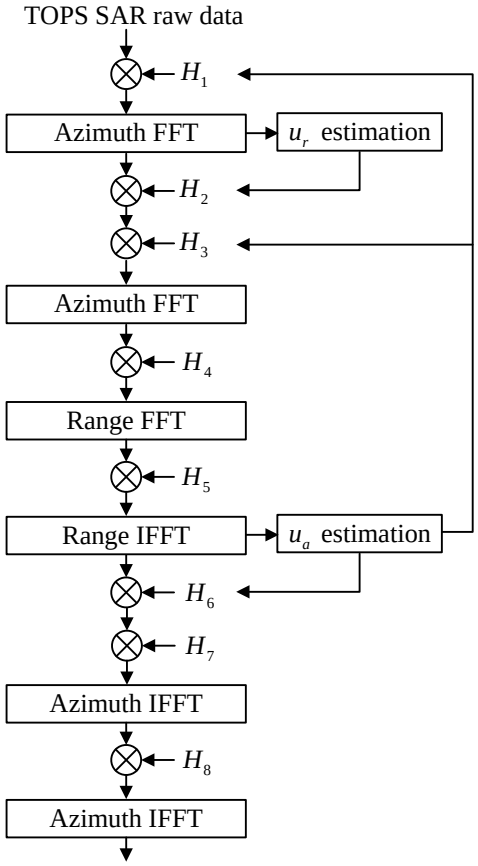

Fig. 4. Block diagram of the proposed imaging approach.

According to the signal model of the moving target, the first multiplied function for moving targets in azimuth pre-filtering is given as follows:

$$H_1(n\cdot\Delta t) = \exp\left[j\pi \frac{2(v_r-u_a)\omega_r}{\lambda}(n\cdot\Delta t)^2 \right], \quad (10)$$

where $n = -I/2,...,0,...,I/2-1$, $\Delta t = 1/\text{PRF}$ is the azimuth time sampling interval, PRF is the pulse

repetition frequency, and I is the number of azimuth samples. As the velocity component u_a is usually unknown before Doppler parameters estimation, $u_a = 0$ is assumed and the value would be updated after the velocity u_a estimation as shown in Fig. 4. After azimuth FT, the Doppler centroid estimation would be taken. As the azimuth time variant Doppler centroid component is removed after multiplying H_1, the Doppler centroid estimation for the resulting raw data of the TOPS mode is the same as the conventional stripmap mode and multiple approaches for the Doppler centroid estimation could be found in [11]. Due to $v_r \gg u_a$, the effect of the unknown velocity u_a on the estimated Doppler centroid of the azimuth center time for SAR raw data collection could be neglected and the estimated velocity $\tilde{u}_r$ could be computed as follows:

$$\tilde{u}_r = -\frac{\lambda \tilde{f}_{ac}}{2}, \tag{11}$$

where $\tilde{f}_{ac}$ is the estimated Doppler center.

Consequently, the following Doppler filter as shown in Fig. 6 is taken to eliminate the out band signal component,

$$H_2(f_a) = \begin{cases} 1, & \tilde{f}_{ac} - B_f/2 \le f_a \le \tilde{f}_{ac} + B_f/2 \\ 0, & \text{otherwise} \end{cases}, \tag{12}$$

where B_f is the azimuth beam bandwidth as shown in Fig. 3. For the azimuth, the second transfer function to be multiplied is:

$$H_3(m \cdot \Delta t') = \exp\left[j\pi \frac{2(v_r - u_a)\omega_r}{\lambda} (m \cdot \Delta t')^2 \right], \tag{13}$$

where $m = -P/2, ..., 0, ..., P/2-1$, $\Delta t' = 1/B_b$ is the azimuth time sampling interval after azimuth pre-filtering, B_b is the Doppler bandwidth of the whole burst in TOPS as shown in Fig. 3, while P is the number of azimuth samples after azimuth pre-filtering and is expressed as follows:

$$P = I + \frac{\mathrm{PRF} \cdot T_f}{A-1}, \tag{14}$$

where T_f is the azimuth synthetic aperture time in the stripmap case for the same exploited azimuth beam interval. Afterwards, the conditional chirp scaling (CS) processor is adopted to implement the following range compression and range cell migration correction (RCMC) processing steps, and the transfer function H_4 and H_5 as shown in Fig. 6 are respectively expressed as follows [11, 12]:

$$H_4(f, f_a) = \exp\left[j\pi \frac{f^2}{k_r (1 + a(f_a))} \right] \cdot \exp\left[j \frac{4\pi r_{ref}}{c} a(f_a) f \right], \tag{15}$$

$$H_5(f_a, \tau; r_{ref}) = \exp\left\{ j \frac{4\pi}{\lambda} r \cdot [\beta(f_a) - 1] - j\pi \frac{f_a^2}{k_{rot}} + j\Delta\phi \right\}, \tag{16}$$

with

$$\beta(f_a) = \sqrt{1 - \left(\frac{\lambda f_a}{2v} \right)^2}, \tag{17}$$

$$a(f_a) = \frac{1}{\beta(f_a)} - 1, \tag{18}$$

$$\frac{1}{k(f_a; r_{ref})} = \frac{1}{K_r} - \frac{2\lambda r \left(\beta^2(f_a) - 1 \right)}{c^2 \cdot \beta^3(f_a)}, \tag{19}$$

$$\Delta\phi = -4\pi \frac{k(f_a; r_{ref}) \cdot [1 - \beta(f_a)]}{c^2 \cdot \beta^2(f_a)} \cdot (r - r_{ref})^2, \tag{20}$$

where f is the range frequency, and r_{ref} is the selected reference range. For the TOPS mode with low geometric resolutions, the effect of the unknown u_a on RCMC could even be neglected. However, the unknown u_a on azimuth compression could not be neglected and would result in the reduced imaging quality. The estimated velocity component $\tilde{u}_a$ is obtained as follows:

$$\tilde{u}_a = \sqrt{ -\frac{\lambda r \tilde{k}_{am}(x, r)}{2} - u_r^2 } - v_r, \tag{21}$$

with

$$\tilde{k}_{am}(x, r) = \left(\frac{\lambda}{2 v_r \omega_r} - \frac{1}{\tilde{k}_a(x, r)} \right)^{-1}, \tag{22}$$

where $\tilde{k}_a(x, r)$ is the estimated Doppler modulation rate after range IFFT. The Doppler modulation rate estimation of the resulting raw data after range IFFT is the same as the one in the stripmap mode. After obtaining the estimated velocity $\tilde{u}_a$, the transfer functions H_1 and H_3 in Fig. 4 should be updated. The azimuth scaling phase function H_6 removes the hyperbolic azimuth phase history for the azimuth data compression, and it is expressed as follows:

$$H_6(r, f_a) = \exp\left[\frac{j4\pi r}{\lambda} \left(\beta(f_a) - 1 \right) \right] \exp\left[j\pi \frac{\lambda}{2v\omega_r} f_a^2 \right]. \tag{23}$$

The multiplied transfer functions H_7 and H_8 with

an azimuth inverse fast Fourier transform (IFFT) step are introduced to implement the azimuth convolution between the compressed azimuth signal and the selected chirp signal to resolve the output back folding in the focused TOPS SAR images. According to (10), the multiplied transfer functions H_7 is expressed as [5, 7]:

$$H_7(f_a) = \exp\left[j\pi \left(n \cdot \Delta f_a\right)^2 / k_d \right], \tag{24}$$

with

$$k_d = \frac{A(r)-1}{A(r)} \cdot \frac{2\left(v_r - u_a\right)^2}{\lambda r}, \tag{25}$$

where $n = -P/2, ..., 0, ..., P/2-1$, $\Delta f_a = 1/T$ is the azimuth time sampling interval, T is the azimuth time duration after azimuth pre-filtering. The final multiplied phase function H_8 in Fig. 4 is easily obtained as follows:

$$H_8(f_a) = \exp\left[j\pi \left(n \cdot \Delta f_a'\right)^2 / k_d \right], \tag{26}$$

with

$$\Delta f_a' = \left| \frac{P \cdot k_d}{\Delta f_a} \right| \tag{27}$$

IV. SIMULATION EXPERIMENT

To validate the proposed imaging approach, simulation experiment on point and distributed targets are carried out and simulation parameters are listed in Table 1.

Table 1: Simulation parameters

Parameters	Value
Carrier frequency	9.65 GHz
Azimuth beam width	0.4º
System PRF	4000Hz
Transmitted pulse duration	20μs
Transmitted pulse bandwidth	20MHz
Sampling frequency	24MHz
Effective velocity	7200m
Burst duration	0.4s
Slant range of imaging center	600km
Azimuth beam rotation rate	2.06º/s

The designed scene including three point targets is shown in Fig. 5, and point target P2 is located at the scene center. Azimuth velocity components u_a of point targets P1, P2 and P3 are 0m/s, 5m/s and 10m/s, respectively, while their range velocity components u_r are 5m/s, 0m/s and 10m/s, respectively.

Figure 6 (a) shows the imaging result of the designed scene, and point targets P1 and P3 are not located at their actual positions due to the range velocity component, which results in an azimuth position shift. Figures 6 (b)~(d) show contour plots of three point targets, which show the well-focused behavior and structure. Resolution, Peak Side Lobe Ratio (PSLR) and Integrated Side Lobe Ratio (ISLR) of three point targets are summarized and listed in Table 2. Both imaging results in Fig. 6 and imaging parameters in Table 2 validate the proposed imaging approach.

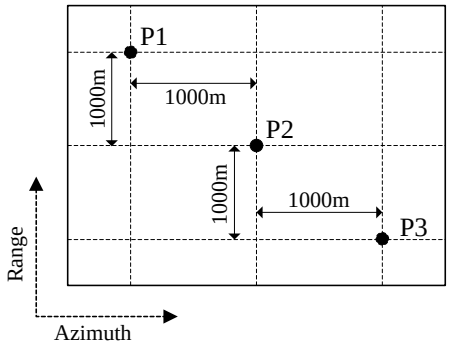

Fig. 5. The designed imaged scene.

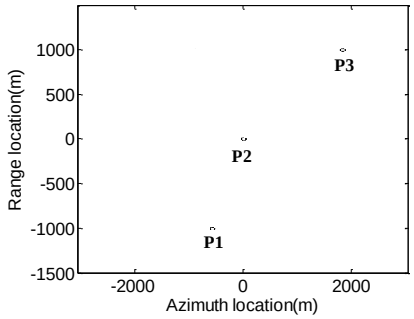

(a) The imaging result

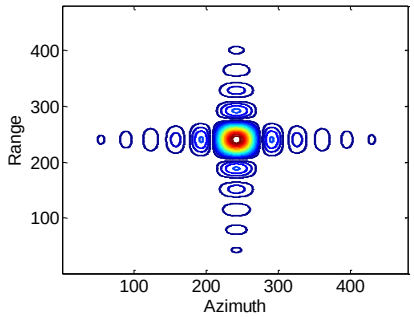

(b) Point target P1

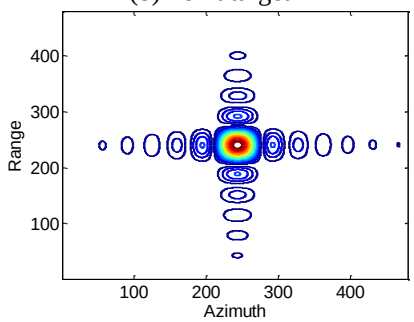

(c) Point target P2

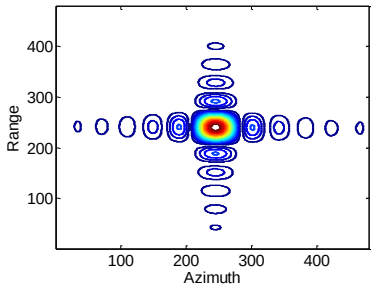

(d) Point target P3

Fig. 6. The imaging results of the designed scene with point targets.

Table 2: Imaging parameters of point targets

		Res (m)	PSLR (dB)	ISLR (dB)
P1	Range	6.65	-13.24	-10.02
	Azimuth	8.02	-13.22	-9.93
P2	Range	6.65	-13.28	-10.10
	Azimuth	8.04	-13.18	-9.96
P3	Range	6.65	-13.23	6.65
	Azimuth	8.04	-13.16	-9.91

To further validate the proposed imaging approach, a simulation experiment on a distributed target is carried out. An electromagnetic modeling of the ship consisting of 45 independent points is designed as shown in Fig. 7 (a), while the velocity components in the range direction and azimuth direction of the designed moving ship are 6m/s and 5m/s, respectively. The raw data of the designed moving ship in TOPS is handled by both the conventional imaging processor in TOPS and the proposed imaging processor. The imaging result handled by the conventional processor shows the defocusing phenomenon as shown in Fig. 7 (b), while it is well focused by the proposed imaging approach as shown in Fig. 7 (c).

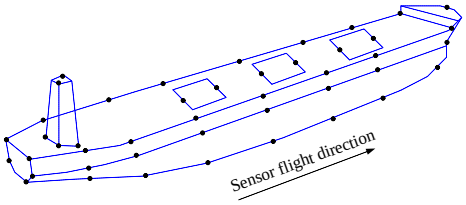

(a) The designed moving ship

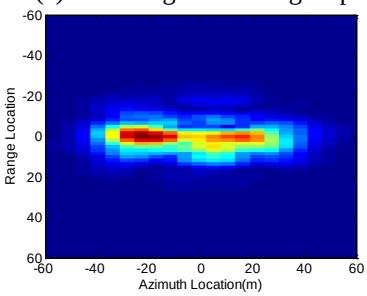

(b) The result by the conventional processor

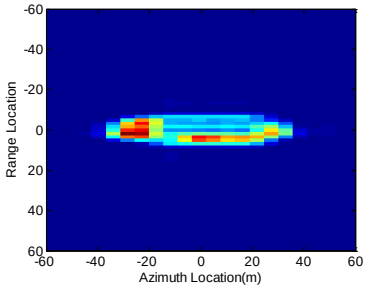

(c) The result by the proposed processor

Fig. 7. The imaging results of the designed moving ship.

V. CONCLUSION

The TOPS mode achieves the wide swath coverage and is attractive for ocean remote sensing. Due to azimuth beam progressive scanning, imaging processors of the TOPS mode are different from other modes. Although multiple TOPS SAR imaging algorithms for fixed targets are proposed in recent years, these algorithms are not very suitable for moving ships in ocean in TOPS. According to the signal model of the moving target in TOPS, we extend the processing ability of the classic TOPS SAR processor to handle the raw data of moving ships. The key points of the proposed imaging approach are the moving target velocity estimation and updating the transfer functions for focusing. Simulation results on both point and distributed targets validate the proposed imaging approach. However, in windy weather conditions, ship motions of roll, yaw, and pitch should be considered during its focusing, and this case requires a more complex imaging processor for moving ships focusing.

ACKNOWLEDGMENT

This work is supported in part by NSF of China (No. 61271177) and in part by the high resolution earth observation system major special project youth innovation foundation of China.

REFERENCE

[1] F. De Zan and A. Monti Guarnieri, "TOPSAR: Terrain observation by progressive scans," *IEEE Trans. Geosci. Remote Sens*., vol. 44, no. 9, pp. 2352-2360, Sep. 2006.

[2] A. Meta, J. Mittermayer, P. Prats, R. Scheiber, and U. Steinbrecher, "TOPS imaging with TerraSAR-X: Mode design and perfomance analysis," *IEEE Trans. Geosci. Remote Sens*., vol. 48, no. 2, pp. 759-769, Feb. 2010.

[3] W Xu, P. Huang, and Y. Deng, "An efficient imaging approach with scaling factors for TOPS mode SAR data focusing," *IEEE Geosci Remote Sens Lett*., vol. 8, no. 5, pp. 929-933, Oct. 2011.

[4] P. Prats, R. Scheiber, J. Mittermayer, A. Meta, and A. Moreira, "Processing of sliding spotlight and

TOPS SAR data using baseband azimuth scaling," *IEEE Trans. Geosci. Remote Sens*., vol. 48, no. 2, pp. 770-780, Feb. 2010.

[5] W Xu, P. Huang, and Y. Deng, "TOPSAR data focusing based on azimuth scaling preprocessing," *Adv. Space Res*., vol. 48, no. 2, pp. 270-277, 2011.

[6] W. Xu, Y. Deng, and R. Wang, "Imaging processor for different spacebarne SAR imaging modes," *IET Elect. Lett*., vol. 48, no. 6, pp. 340-342, Mar. 2012.

[7] W. Xu, P. Huang, Y. Deng, and R. Wang, "TOPS-mode raw data processing using chirp scaling algorithm," *IEEE Journal of Selected Topics in Applied Earth Observations and Remote Sensing*, vol. 7, no. 1, pp. 235-246, 2014.

[8] S. Zhu, G. Liao, Y. Qu, Z. Zhou, and X. Liu, "Ground moving targets imaging algorithm for synthetic aperture radar," *IEEE Trans. Geosci. Remote Sens*., vol. 49, no. 1, pp. 462-477, Jan. 2011.

[9] J. K. Jao, "Theory of synthetic aperture radar imaging of a moving target," *IEEE Trans. Geosci. Remote Sens*., vol. 39, no. 9, pp. 1984-1992, Sep. 2001.

[10] W. Zhou, J.-T. Wang, H. W. Chen, and X. Li, "Signal model and moving target detection based on MIMO synthetic aperture radar," *Progress In Electromagnetics Research*, vol. 131, pp. 311-329, 2012.

[11] I. G. Cumming and F. H. Wong, *Digital Processing of Synthetic Aperture Radar Data: Algorithms and Implementation*, Artech House, Norwood, MA, 2005.

[12] A. Moreira, J. Mittermayer, and R. Scheiber, "Extended chirp scaling algorithm for air- and spaceborne SAR data processing in stripmap and ScanSAR imaging modes," *IEEE Trans. Geosci. Remote Sens*., vol. 34, no. 5, pp. 1123-1136, Sep. 1996.

Hongbo Mo, Ph.D. student of Beijing University of Posts and Telecommunications. His research interests include signal processing, wireless telecommunication and Internet of Things.